Journal of Materials Chemistry A

Accepted Manuscript

This is an *Accepted Manuscript*, which has been through the Royal Society of Chemistry peer review process and has been accepted for publication.

Accepted Manuscripts are published online shortly after acceptance, before technical editing, formatting and proof reading. Using this free service, authors can make their results available to the community, in citable form, before we publish the edited article. We will replace this *Accepted Manuscript* with the edited and formatted *Advance Article* as soon as it is available.

You can find more information about *Accepted Manuscripts* in the Information for Authors.

Please note that technical editing may introduce minor changes to the text and/or graphics, which may alter content. The journal's standard Terms & Conditions and the Ethical guidelines still apply. In no event shall the Royal Society of Chemistry be held responsible for any errors or omissions in this *Accepted Manuscript* or any consequences arising from the use of any information it contains.

ROYAL SOCIETY OF CHEMISTRY

www.rsc.org/materialsA

Journal of Materials Chemistry A

Dynamic Article Links►

Cite this: DOI: 10.1039/c0xx00000x

ARTICLE TYPE

www.rsc.org/xxxxxx

Enhanced performance in hybrid perovskite solar cell by modification with spinel lithium titanate

Jiangwei Li, Wenzhe Li, Haopeng Dong, Nan Li, Xudong Guo, Liduo Wang*

Received (in XXX, XXX) XthXXXXXXXXX 20XX, Accepted Xth XXXXXXXXX 20XX

DOI: 10.1039/b000000x

Lithium salts have been important additives to the hole-transport materials of solid-state hybrid perovskite solar cells to achieve higher hole mobility. However, the observed intercalation of Li^+ into TiO_2 was demonstrated to decrease the open-circuit voltage (V_{OC}) of the cells. In this work, spinel lithium titanate $Li_4Ti_5O_{12}$ (LTO) was used to alleviate this issue by consuming Li^+ prior to contact of Li^+ with TiO_2 at the interface between sensitized TiO_2 and hole-transport layer through chemical insertion of Li^+ into LTO. Raman and X-ray photoelectron spectroscopy results confirmed the insertion of Li^+ into LTO. A Li^+ insertion peak in cyclic voltammetry and the increased density of states of TiO_2 revealed the role of LTO as a Li^+ separator to protect the TiO_2 photoanode, providing the mechanism of V_{OC} increase for LTO modification. Electrochemical impedance spectroscopy revealed that LTO modification markedly reduced carrier recombination, improving the fill factor of the devices. Overall, the conversion efficiencies of devices was significantly increased with a maximum efficiency of 15.1% by addition of LTO. The strategy of using LTO as a multifunctional modifier broadens the scope of interface engineering in solar cells.

1 Introduction

Methylammonium lead halide perovskite solar cells (PSCs) have attracted great attention from material scientists and become a research hotspot in recent years. As great effort to develop the excellent light-harvesting characteristics of perovskite materials and simplify fabrication has been expended, the efficiencies of PSCs keep soaring.[1-9] To date, a highest power conversion efficiency (PCE) of 19.3% has been achieved in solid-state PSCs by controlling fabrication conditions and interface engineering.[9] Such advances in performance make solid-state PSCs a candidate for next-generation solar cells[10,11]

An important additive to the hole-transport layer (HTL) of solid-state PSCs is lithium salt, typically bis(trifluoromethane)sulfonimide lithium (Li-TFSI), which is used to increase conductivity and hole mobility.[3,7-9,12,13] Adding Li-TFSI increases the conductivity of the commonly used hole-transport material 2,29,7,79-tetrakis-(N,N-di-p-methoxyphenyl-amine)-9,99-spirobifluorene (spiro-MeOTAD) by about three orders of magnitudes, guaranteeing efficient hole transfer.[13] However, research on dye-sensitized solar cells has shown that Li^+ in the electrolyte can easily intercalate into mesoporous TiO_2 films,

$$x\,\mathrm{Li}^+ + x\,e^-_{\mathrm{TiO_2}} + \mathrm{TiO_2} \rightarrow \mathrm{Li}_x\mathrm{TiO_2}, \quad (1)$$

which increases the number of trap states, broadens the density of states (DOS) and lowers the energy level of the conduction band (CB) of TiO_2 anode, thereby decreasing voltage potential.[14-18] During solution-coating of hole-transport materials, Li^+ would inevitably contact the mesoporous TiO_2 surfaces, decreasing the open-circuit voltage (V_{OC}) of devices through the same mechanism. This assumption is supported by the results of Snaith *et al*.[13] In addition, the role of Li^+ is not exclusive. There have been works on Li^+ replacement involving compounds like HTFSI, BuPyIm-TFSI and AgTFSI.[19-21] Therefore, strategies to both retain hole-transfer performance in the HTL and separate Li^+ from TiO_2 at the sensitized TiO_2/HTL interface should be considered.

In this work, we use spinel lithium titanate $Li_4Ti_5O_{12}$ (LTO) to modify the interface between perovskite layer and HTL to prevent contact of Li^+ with exposed TiO_2 while retaining its function of ensuring hole transpot in HTL. LTO is an anode material for lithium ion batteries. Li^+ can be inserted into LTO both electrochemically and chemically, while the expansion of unit cell lattice of LTO is negligible upon insertion of lithium due to the "zero-strain" property of LTO.[22-25] We confirm a chemical Li^+ insertion reaction between Li-TFSI and LTO by Raman spectroscopy and X-Ray photoelectron spectroscopy (XPS). From interpretation of cyclic voltammetry (CV) and the change of the DOS of TiO_2 after LTO modification, we propose a Li^+-separation mechanism for V_{OC} increase. Electrochemical impedance spectroscopy (EIS) shows that LTO modification also markedly improves the fill factor (FF) of the device because of reduced carrier recombination. Overall, LTO modification

Journal of Materials Chemistry A Accepted Manuscript

markedly raises the conversion efficiencies of solar cells to reach a maximum efficiency of 15.1%.

2 Experiment

2.1 Solar cell fabrication

All chemicals were used as received. Methylammonium iodide (CH_3NH_3I) was synthesized by mixing methylamine (27.8 mL, 40% in methanol, Alfa Aesar) and hydroiodic acid (30 mL, 57% wt% in water, Alfa Aesar) in a 250-mL round-bottom flask, and stirring the mixture in an ice-water bath for 2 h. The yellowish raw product obtained by evaporating the solvent was recrystallized three times from a mixture of diethyl ether and ethanol. After filtration, the solid was collected in a dark container and dried at 60 ℃ in a vacuum oven overnight. On the initial stage of optimizing the concentration of LTO solution, the compact TiO_2 layer was prepared by spin-coating the TiO_2 precursor solution, which was prepared by mixing titanium(IV) isopropoxide (1 mL, 99.999%, Sigma Aldrich) with 2-methoxyethanol (5 mL, 99%, Alfa Aesar) and ethanolamine (0.5 mL, 98%, Alfa Aesar), at 3000 rpm for 30 s on a cleaned FTO glass, followed by a subsequent heating at 500 ℃ for 60 min. With the optimized results, we upgraded the compact TiO_2 layer to a 15 nm one with atomic layer deposition methods (Beneq TFS 200) for further efficiency improvement. Titanium dioxide (TiO_2) was deposited at 150 ℃ using titanium tetrachloride ($TiCl_4$) and H_2O as Ti and O precursors, respectively. The mesoporous TiO_2 film was then deposited by spin-coating a treated TiO_2 paste (18NR-T, Dysol) at 7000 rpm for 30 s, followed by sintering at 500 ℃ in a tube furnace for 1 h and naturally cooling to room temperature. $CH_3NH_3PbI_3$ was prepared in a glovebox filled with dry air by the sequential deposition method reported previously.[7] First, PbI_2 (463 mg L^{-1}, 99.9985%, Alfa Aesar) in anhydrous N,N-dimethylformamide (99.9%, Sigma Aldrich) was spin-coated on the substrates at 5000 rpm for 60 s. After heating at 70 ℃ for 30 min and cooling, the film was immersed in the as-prepared CH_3NH_3I (10 mg L^{-1}) in 2-propanol (99.9%, Sigma Aldrich) for 120 s and then rinsed with 2-propanol. The $CH_3NH_3PbI_3$ layer was formed after sintering for 30 min at 70 ℃. The LTO-treatment process was implemented as follows: LTO (18 mg, Tianjin Lishen Co, China.) was dispersed in chlorobenzene (3 mL, 99.8%, Sigma Aldrich) and then filtered through a 220-nm filter to give a saturated LTO solution. LTO solutions of different concentration were then prepared by dilution of the saturated one. LTO treatment involved spin-coating the required diluted LTO solution on the prepared $CH_3NH_3PbI_3$ film at 7000 rpm for 30 s. To prepare the HTL, spiro-MeOTAD (73 mg, Luminescence Technology Corp.), Li-TFSI (9.1 mg, 99.95%, Sigma Aldrich) and 4-*tert*-butylpyridine (tBP, 37.5 μL, 96%, Sigma Aldrich) were added to chlorobenzene (1 mL) to form a hole-transport material solution and then spin-coated at 4000 rpm for 30 s. Complete devices without encapsulation were fabricated by thermal evaporation of 60 nm of Au as the counter electrode. The active area of each device was 0.09 cm^2.

2.2 Characterization.

Raman spectra (Horiba LabRAM HR Evolution) were recorded using the green line (514.5 nm) of an argon laser (Spectra Physics). Mass ratio of element Li, S, Ti were performed by Inductively Coupled Plasma Optical Emission Spectra (ICP-OES, Thermo IRIS intrepid II). UV−vis spectra were carried out on a Hitachi U-3010 UV−vis spectrometer. Measurements of solutions were taken in a 1 cm glass cuvette placed in a cuvette holder integrated within the setup. XPS (ESCALAB 250Xi, Thermo Scientific) was measured and analyzed by XPSPeak software. Atom force microscopy (AFM) was performed with a scanning probe microscope (SPA-400, Seiko Instruments, Japan). Transmission Electron Microscopy (TEM) images were taken on a Hitachi HT7700 transmission electron microscope with an acceleration voltage of 100 kV. TEM grids were dipped in the relative solutions to deposit LTO nanosheets onto the film. CVs, photocurrent–voltage (J-V) curves, incident photon-to-electron conversion efficiency (IPCE) and EIS (0.1 to 10^5 Hz) were measured by an electrochemical workstation (Zahner, CIMPS). J-V curves were obtained with a scan speed of 50 mV/s from 1 to 0 V under 1-sun illumination conditions, AM 1.5 100 mW cm^{-2} simulated sunlight (ORIEL 81193, 1000 W Xe light source) calibrated with an NREL-calibrated silicon solar cell.

3 Results and discussion

3.1 Li^+ effect and insertion reaction with LTO

To determine the effect of Li-TFSI on the V_{OC} of perovskite-based solid-state solar cells, we fabricated cells with different Li-TFSI contents in the HTL and examined their V_{OC}, as shown in Figure 1a. As the concentration of Li-TFSI increased, V_{OC} of the devices decreased. A reasonable explanation could be that inevitable contact between Li^+ and the TiO_2 mesoporous film occurred during the dipping and spin-coating processes. Large perovskite grains in the capping layer created a rough surface, and incomplete covering of the perovskite layer exposed surfaces of the TiO_2 film,[7] making it easy for Li^+ to reaction with TiO_2. A schematic diagram of the change of the DOS of TiO_2 with Li^+ concentration is presented in Figure 1b to illustrate the effect of Li^+ intercalation.[18] The broadening of the DOS of TiO_2 led to a lower CB edge and thereby a lower V_{OC}. The optimum Li-TFSI additive content should take account of both the increase of J_{SC} and the decrease of V_{OC} to ensure an overall conversion efficiency enhancement. Once we take steps to minimize the decrease of V_{OC}, we shall obtain a higher efficiency.

For this purpose, we added LTO to our system. As an anode material for lithium ion batteries, LTO exhibits Li-insertion capability and lattice stability as we desire. Moreover, chemical Li^+ insertion into LTO and superior stability of the reaction

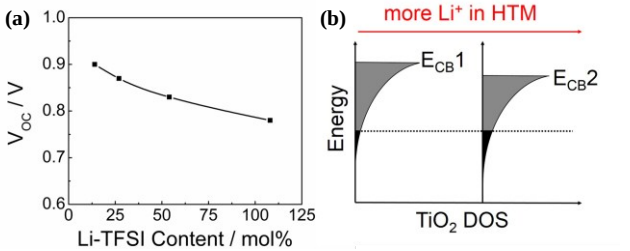

Figure 1. (a) V_{OC} characteristics with different Li-TFSI contents in HTL, (b) Schematic of the change of DOS of TiO_2 with more Li^+ in HTL.

Journal of Materials Chemistry A Accepted Manuscript

This journal is © The Royal Society of Chemistry [year]

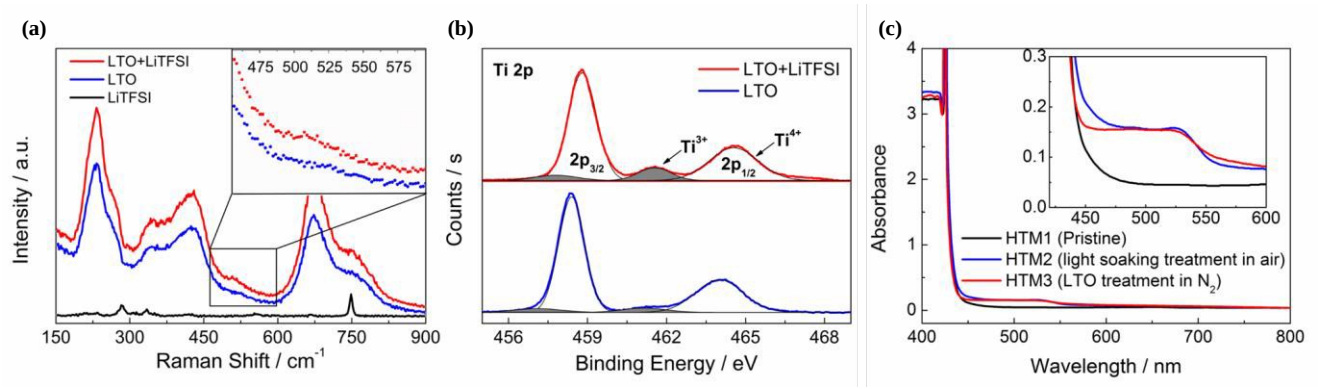

Figure 2. (a) Raman spectrum and (b) Ti 2p XPS of LTO after reaction with LiTFSI in HTM solution, (c) Absorption spectra of HTM1 (pristine HTM solution in N_2), HTM2 (HTM solution after 10 min light soaking treatment in air) and HTM3 (centrifuged HTM solution after reaction with LTO powder in N_2). Insets in (a) and (c) show magnified images of the Li-O stretching vibration regions and the oxidized spiro-MeOTAD peak at 520 nm.

products have been demonstrated.[23] We investigated the insertion of Li^+ from LiTFSI into LTO by Raman spectra (Figure 2a). After mixing LTO with the hole-transport material solution, which simulated the reaction environment during modification, we washed the product three times with chlorobenzene to remove other components. The Raman spectra exhibit peaks in the wavelength range of 400–550 cm^{-1} from the Li-O stretching vibration in the LiO_4 tetrahedron. The observation of a peak at 509 cm^{-1} was consistent with coupling of different mode of Li-O stretching vibration when Li^+ was inserted into the LTO lattice.[23,24] However, the intensity of this peak was relatively weak. Given that the measurement depth of Raman spectroscopy is of submicron order, we presumed that Li^+ insertion mainly happened at the LTO surface rather than the bulk area, reducing the intensity of Raman results.

Considering that XPS is usually used to obtain information of crystal surface area with a depth of several nanometers, we took XPS measurements as further evidence to confirm the findings suggested by Raman results. The XPS data provided clear evidence for the change of valence state of Ti after Li^+ inserted. Figure 2b showed the Ti 2p spectrum with peaks at 458.37 and 463.98 eV from Ti(IV), and 457.12 and 461.17 eV from Ti(III).[26] The $TFSI^-$ counterion was inevitably adsorbed on the surface despite washing, proved by the appearance of a F 1s peak in Fig. S1. The inductive effect of the negatively charged $TFSI^-$ led to a slightly positive shift of the binding energy. Ti(IV) is the theoretical valence state of LTO. The amount of Li^+ is always excess in the lattice causing Ti(IV) to be partially reduced to Ti(III), which reflects the amount of exotic Li^+ in the LTO lattice. We performed data fitting of the XPS results based on the Gauss function to determine the integrated peak areas. The calculated peak areas revealed that the molar ratio of Ti(III) was 7% and 12% before and after the reaction, respectively. The difference of nearly 5% is large enough to speculate that Li^+ reacted easily on the crystal surface of LTO and the results gave a calculated reaction molar ratio of 1:0.6.

Moreover, we performed ICP-OES measurements on the reacted LTO and UV-Vis absorption spectra of the centrifuged HTM solution after reaction with LTO to investigate the detailed reaction mechanism.

The results of ICP-OES revealed that after reaction, the molar ratio of Li/Ti increased from 0.823 to 0.833, indicating a change of element composition from $Li_{4.12}Ti_5O_{12}$ to $Li_{4.18}Ti_5O_{12}$ (Table. S1). That meant an overall molar ratio of inserted Li should be 1:0.06. Compared with information obtained from Raman spectra and XPS, we believed that the insertion reaction of Li^+ mainly happens on the very surface of LTO. This conclusion provided information that if we applied LTO with structure with large surface area like nanosheet etc., we would obtain a much higher reaction activity of Li^+ insertion. Since we succeeded in preparing and applying LTO nanosheets, which will be discussed later, it would be more accurate to use the reaction molar ratio of 1:0.6 obtained from XPS because the thickness of LTO nanosheet is more close to the measurement depth of XPS.

After reaction of LTO powder with LiTFSI, we collected the HTM solution by centrifugation and found it had turned into orange from original yellowish. Then we performed UV-Vis absorption spectra and detected a peak maxima located at around 520 nm. This absorption band results from the formation of oxidized spiro-MeOTAD cation radical.[27] It is well known that the photo-oxidation of spiro-MeOTAD needs oxygen as p-dopant,[13,28] which is also supported by the absorption spectra of HTM solutions stored in N_2 and light-soaking treated in air (Figure 2c). Since the reaction of LTO took place in N_2, we believed that the reduction reaction of Ti(IV) by Li^+ insertion demonstrated before was chemically driven by the oxidation of spiro-MeOTAD. And the anion $TFSI^-$ could be the counter ion to stabilize the oxidized spiro-MeOTAD cation radical as reported.[13] Our demonstrated reaction molar ratio was 1:0.6, which differed from the ratio of 1:1.77 previously reported.[23] And based on the analysis before, we attributed the reactivity difference to different reaction driving force. Finally, we presented Li^+ insertion reaction as follow.

$$0.6\,Li^+ + 0.6\,e^- + Li_4Ti_5O_{12} \rightarrow Li_{4.6}Ti_5O_{12} \quad (2\text{-}1)$$

$$\text{spiro-MeOTAD} + TFSI^- \rightarrow \text{spiro-MeOTAD}^{\bullet+}TFSI^- + e^- \quad (2\text{-}2)$$

Inspired by the fact that the surface areas exhibited higher Li^+ insertion activity, we then filtered the saturated LTO solution to constrain the crystal size and obtain larger specific surface areas. The measured solid content of the saturated solution was 55 $mg\,L^{-1}$. After coating the LTO solution on the silicon substrate, we used AFM to observe the morphology and size distribution of LTO particles (Figure 3a-c). The determined particle diameter distribution revealed the LTO particles had a transverse width of 115±13 nm and vertical height of 14±4 nm, suggesting LTO had

Journal of Materials Chemistry A Accepted Manuscript

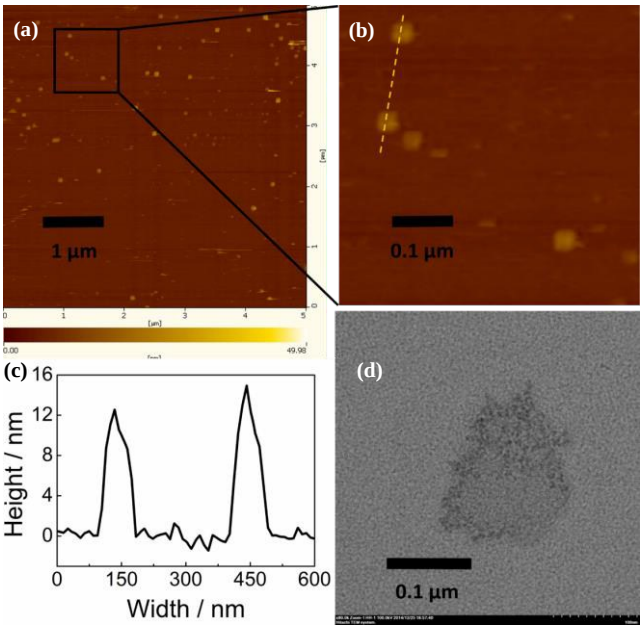

Figure.3 (a) AFM image of deposited LTO nanosheets on silicon substrate, (b) the corresponding magnified image with height information on the orange dash line depicted in (c), (d) TEM image of LTO nanosheets.

a nanosheet structure and coinciding with the size of pores of the filters we used. The TEM image shown in Figure 3d gave the same size information. Also, the sample exhibited a relatively low contrast, indicating a rather thin layer. Although the LTO particles were not monodisperse, such an easy way to obtain nanosheet structure was exciting, because not only was the method simple and repeatable, but the as-prepared LTO nanosheets also exhibited large surface area to give higher Li^+ insertion activity. Unlike the smooth surface of the silicon substrate, the perovskite layer was so rough that flowing LTO nanosheets should be trapped around the $CH_3NH_3PbI_3$ crystal boundaries, where TiO_2 was most likely to be exposed.

3.2 Photovoltaic performance improvement with LTO modification

To demonstrate our assumption that V_{OC} would be increased by addition of LTO, we measured the photovoltaic characteristics of devices treated with different concentration of LTO solutions (Figure 5a). As the concentration of LTO solution increased, V_{OC} of the devices were raised, while J_{SC} and FF increased initially and then decreased. With an optimized LTO solution concentration of 14 mg L^{-1}, the efficiencies of the PSCs were markedly improved from 8.6% to 10.8%. We then upgraded the original spin-coated compact TiO_2 layer to a 15-nm film prepared by ALD methods, which substantially improved the overall conversion efficiency to 13.4% with a maximum PCE of 15.1% compared to the control groups with efficiencies of 11.5% (histogram of efficiencies shown in Figure S3). The schematics of device architecture and the relative energy levels of each layer of the perovskite solar cells are shown in Figure 4.

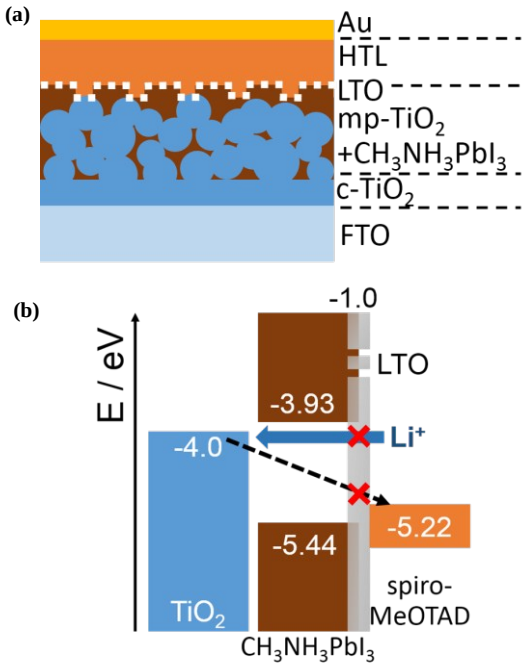

Figure. 4 Schematic of (a) device architecture and (b) the relative energy levels of each layer of the perovskite solar cells

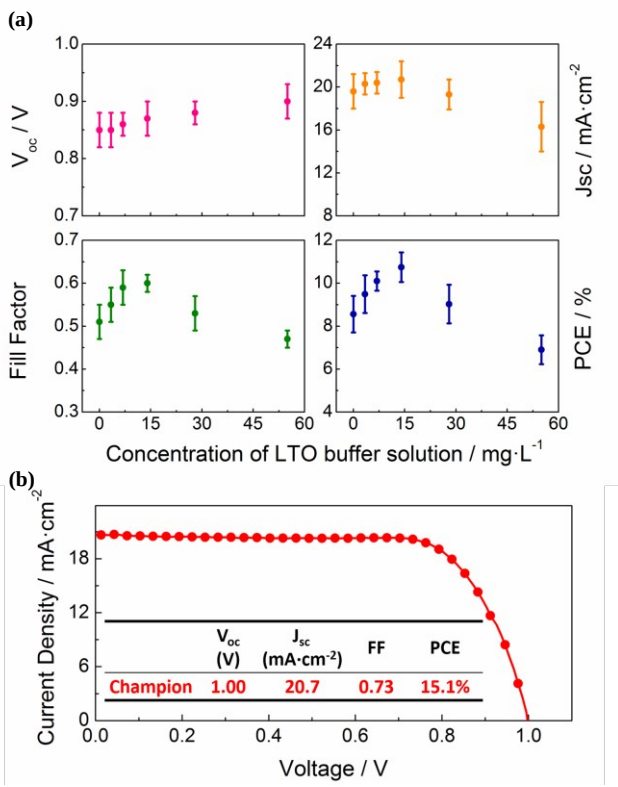

Figure 5. (a) Photovoltaic characteristics for PSCs with LTO modification of different concentration (statistics of data for 10 batches of devices). (b) J-V curve of the champion device with LTO modification. Insert table shows the corresponding photovoltaic characteristics. There are differences of compact TiO_2 layer preparation methods between (a) and (b) as stated in the experiment part.

Journal of Materials Chemistry A Accepted Manuscript

This journal is © The Royal Society of Chemistry [year]

3.2.1 LTO as a Li^+ separator to increase V_{OC}

To further understand the correlation between the chemical Li^+ insertion reaction of LTO and subsequent increase of V_{OC}, we need to study the Li^+ insertion properties of the LTO nanosheets and the change of DOS of TiO_2 caused by LTO modification. Figure 6 displays the first two scans of cyclic voltammetry of the TiO_2 mesoporous working electrodes treated with and without LTO nanosheets in 0.1 M $LiClO_4$/acetonitrile. Both electrodes showed a cathodic peak from -0.7 V corresponding to Li^+ intercalation into the TiO_2 electrode.[15] Compared with the pristine TiO_2 working electrode, a broad cathodic peak emerged from -0.2 V in the first scan of the LTO-treated electrode, indicating a rather active reductive reaction, which disappeared after the first cycle. An identical peak was observed in the CV of a LTO working electrode, so this peak represents a characteristic reaction of LTO (Figure S4). Two sequential cathodic peaks at -1.1 and -1.4 V were consistent with the electrochemical insertion of Li^+, probably for two different routes of Li^+ diffusion.[29] This allowed us to attribute the characteristic peak of LTO electrode at around -0.2 V to the electrochemically driven Li^+ insertion

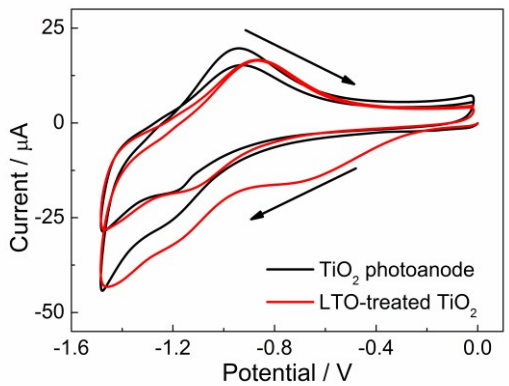

Figure 6. First two scans of CVs with TiO_2 (black) or LTO-treated TiO_2 (red) working electrodes, Pt counter electrode and Ag reference electrode in 0.1M $LiClO_4$/acetonitrile at a scan speed of 50 mV/s. Arrows show the scan directions.

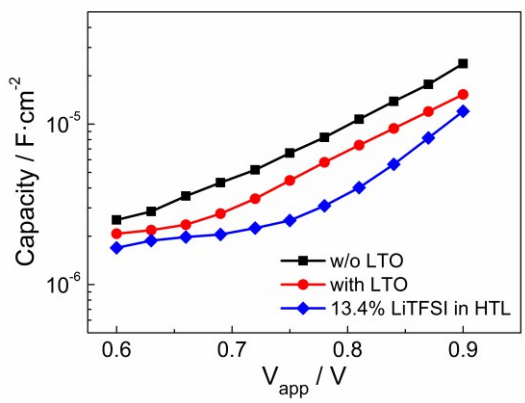

Figure 7. Chemical capacitance extracted at an intermediate frequency of 1000 Hz from EIS of: pristine device (black), with LTO modification (red) and with low LiTFSI molar ratio of 13.4% in the HTL (blue), performed under one sun illumination condition with a 0.8 V bias voltage.

reaction, coinciding with our observation of the spontaneous chemical insertion of Li^+ into LTO. We concluded that LTO nanosheets acted as Li^+ separators, functioning when they were deposited onto the bare regions of TiO_2 and preventing Li^+ from intercalating into TiO_2 despite their tendency to do so even at low voltage generated by the fabricated PSCs under indoor light intensity. Considering the decrease of V_{OC} caused by Li^+ intercalation was caused by increasing traps and broadening the DOS of TiO_2, we determined the change of the DOS distribution of TiO_2 by extracting the chemical capacitance from the intermediate frequency region of EIS measurements, as shown in Figure 7. Chemical capacitance describes the capacity for charge carrier accumulation,[30-32] so the capacitance of the TiO_2/perovskite interface obtained from the corresponding frequency region in EIS describes the carrier accumulation in TiO_2, reflecting its exponential DOS.[31] Reducing the content of Li^+ in the HTL decreased the capacitance of TiO_2, indicating a higher DOS, which coincided with a higher TiO_2 CB edge and increased V_{OC}. Intercalation of Li^+ into TiO_2 caused DOS broadening and deepening because it increased the number of trap states. This was the main reason for the observed lower capacitance in the system with a small amount of Li^+. LTO modification caused a similar decreasing trend of the TiO_2 capacitance. Because volume shrinkage during crystallization and solvent evaporation is hard to control especially for $CH_3NH_3PbI_3$ with mesoporous TiO_2 scaffold, there were numerous exposed regions on the TiO_2 surfaces that directly contacted the HTL, where a large amount of Li^+ could unrestrictedly intercalate into TiO_2. We speculate that the LTO nanosheets were deposited on these regions during the coating process because these regions exhibited valley-like morphology. The protective effect of LTO nanosheets on the TiO_2 electrode as Li^+ separators is a plausible explanation for the observed higher TiO_2 DOS and V_{OC} of the LTO-modified devices.

In addition, we used the reacted LTO (r-LTO) as modification materials to study the effect of the amount of inserted Li^+ on the photovoltaic performance and the comparison results are listed in Table S2. Compared with the control group, the r-LTO modified devices exhibited a slightly higher V_{OC}, which confirmed a much higher Li^+ blocking efficiency of the pristine LTO and provided support for our choice of LTO as Li^+ separators.

3.2.2 LTO modification to reduce recombination

Among all the photovoltaic parameters considered, FF was prominently improved with LTO modification. FF determines the maximum power generated from a solar cell and is strongly affected by the series resistance and shunt resistance of the device. FF rapidly decreases when there are defects and severe carrier recombination. As the concentration of the LTO solution increased, the FF increased initially and then decreased. Considering other modification materials reported before,[33,34] we speculated that the LTO nanosheets acted as an insulating layer and reduced carrier recombination at the sensitized TiO_2/HTL interface. The CB energy of LTO is -1.0 eV,[35] which is much higher than the CB energy of $CH_3NH_3PbI_3$ and HOMO energy of HTM, indicating the ability of LTO modification materials to reduce carrier recombination. Schematic of the relative energy levels is shown in Fig. 4(b). Moreover, the observed decrease of dark current in Figure 8c is consistent with this hypothesis,

Journal of Materials Chemistry A Accepted Manuscript

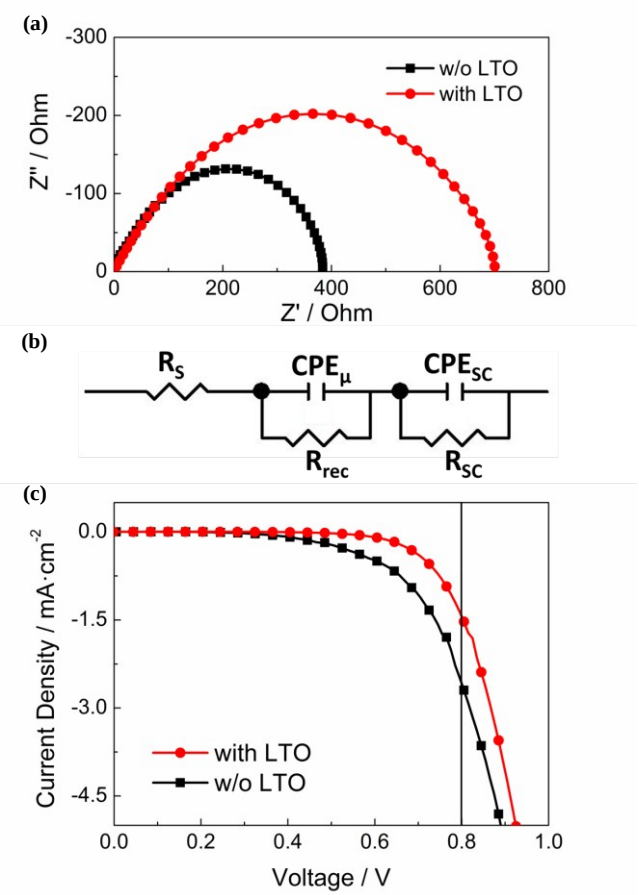

Figure 8. (a) Nyquist plots of EIS measurements under dark condition with a 0.8 V bias voltage (b) Equivalent circuit model used for EIS analysis (R_s and R_{rec} are the series resistance and recombination resistance of device, CPE_μ is the chemical capacitance of films and R-CPE_{sc} is the impedance of selective contacts), (c) Dark current curve of devices with (red) and without (red) LTO modification.

because it benefited from less undesired shunting paths and dark reaction.

To clarify the effect of LTO modification on carrier recombination, we used EIS to observe the recombination resistance of the solar cells. Figure 8b depicts the equivalent circuit used to fit the Nyquist plots from EIS measurements. R_{rec} represents the recombination resistance, which is inversely related to the recombination rate. The second R-CPE feature depicts the impedance of selective contacts (sc), including compact TiO_2 for electron-selective contacts and HTL for hole-selective contacts.[36,37] Under dark conditions (Figure 8a), R_{rec} was reflected by the second arc at lower frequencies, while the first arc at high frequencies was partially presented and almost indistinguishable.[38,39] For PSCs, recombination mainly occurs at the functional layer interface where electrons in the CB of TiO_2 or perovskite layer recombine with holes in the highest occupied molecular orbital (HOMO) level of the HTL. After LTO modification, the recombination resistance almost doubled, indicating an effective reduction of carrier recombination. Although the LTO nanosheet layer increased R_{rec} between the perovskite film and HTL benefited from its inherent insulating property, it would undoubtedly hinder charge-carrier transfer as well. In view of both recombination retarding and carrier-transport resisting caused by LTO modification, we need to find a balance point to achieve an overall benefit in efficiencies, which was also proved by the variation of FF with LTO concentration. The optimized concentration of LTO with the largest enhancement in both FF and J_{SC} was determined to be 14 mg L^{-1}. When a higher concentration of LTO solution was used, the forward carrier transport was severely impeded, triggering a large decrease in both FF and J_{SC}. In contrast, a lower concentration of LTO had relatively weak ability to retard recombination. Besides, we noticed that the r-LTO modified devices exhibited similar FF to the LTO modified ones, indicating their similar abilities of retarding carrier recombination with the same contents, i.e. the same degree of perovskite coverage on TiO_2 films. However, considering the r-LTO modification provided little improvement in V_{OC}, we believe our selection of Li^+ intercalating materials over insulating materials without any Li uptake ability was wise, because the former ones block Li^+ more efficiently to achieve a higher V_{OC}.

While V_{OC} and FF were increased by the proposed Li^+-separation mechanism and prominent reduction in carrier recombination, respectively, J_{SC} was increased by a negligible amount. To overcome the decrease of V_{OC} caused by Li^+ intercalation into TiO_2, the CB edge of TiO_2 would shift upwards. Then the energy difference between the CB edge of TiO_2 and that of perovskite would decrease, giving a smaller free energy change ($-\Delta G_{inj}$) and reducing the electron injection efficiency.[17] This would reduce J_{SC}, contrary to our observations. However, J_{SC} was nearly unaffected benefited from LTO effectively retarding carrier recombination (Figure 5a).

One may wonder whether the V_{OC} increase is attributed to the reduced recombination process rather than the proposed Li^+-separation mechanism. To address this issue, we need further insight into the behavior of V_{OC}. Insulating materials typically retard recombination with a slight increase in V_{OC}, as the r-LTO modified devices exhibited. When a larger amount of materials are used, V_{OC} will decrease along with FF and J_{SC}, which is attributed to the decrease of I_{SC}.[33] On the contrary, as the concentration of LTO solution increased, V_{OC} kept increasing, indicating a continuous effect on the modified devices (Figure 5a). This behavior can be ascribed to LTO protection, because a continuously decreasing amount of Li^+ comes in contact with TiO_2 as the concentration of LTO solution increases.

In general, LTO nanosheets exhibit sufficient Li^+ uptake ability to protect TiO_2 from Li^+ intercalation, superior crystal lattice stability to sustain effect during energy conversion and inherent insulating properties to achieve less carrier recombination. The strategy of using LTO as multifunctional modifier should be paid attention because of its potential in solar-cell applications.

4 Conclusions

We demonstrated that decrease of V_{OC} in hybrid perovskite solid-state solar cells is caused by Li^+ intercalation into TiO_2. However, this effect could be largely overcome by protecting the TiO_2 anode from Li^+ contact by addition of LTO. Raman spectra and XPS results confirmed the chemical Li^+ insertion reaction between LiTFSI and LTO. Then we prepared size-constrained LTO nanosheets by a simple physical exfoliation method of

Journal of Materials Chemistry A Accepted Manuscript

This journal is © The Royal Society of Chemistry [year]

filtering and confirmed their roles as Li^+ separators to protect the TiO_2 photoanode from Li^+ intercalation. Less contact of Li^+ with TiO_2 resulted in fewer trap states in the TiO_2 films, leading to higher TiO_2 DOS and increased V_{OC} of the devices with LTO modification. The interaction between Li^+ and the perovskite layer remains unclear, and we are making efforts to study it. LTO nanosheets themselves acted as insulating layer, reducing carrier recombination and improved FF. The optimized concentration of LTO of 14 mg L^{-1} was obtained, which gave a marked enhancement of performance and a maximum PCE of 15.1%. In this study, a feasible strategy of interface modification in solid-state hybrid perovskite solar cells was developed, providing the promise of multiple function of the interface modification methods.

Acknowledgements

This work is supported by the National Natural Science Foundation of China under Grant no. 51273104.

Notes and references

Key Lab of Organic Optoelectronics & Molecular Engineering of Ministry of Education, Department of Chemistry, Tsinghua University, Beijing 100084, China. Fax: (008610) 62795137 Tel: (008610) 62788802. E-mail: chldwang@mail.tsinghua.edu.cn.

1 Kojima, A.; Teshima, K.; Shirai, Y.; Miyasaka, T. *J. Am. Chem. Soc.*, **2009**, *131*, 6050-6051.
2 Im, J. H.; Lee, C. R.; Lee, J. W.; Park, S. W.; Park, N. G. *Nanoscale*, **2011**, *3*, 4088-4093.
3 Kim, H. S.; Lee, C. R.; Im, J. H.; Lee, K. B.; Moehl, T.; Marchioro, A.; Moon, S. J.; Humphry-Baker, R.; Yum, J. H.; Moser, J. E.; Gratzel, M.; Park, N. G. *Sci Rep*, **2012**, *2*, 591 – 597.
4 Lee, M. M.; Teuscher, J.; Miyasaka, T.; Murakami, T. N.; Snaith, H. J. *Science*, **2012**, *338*, 643-647.
5 Stranks, S. D.; Eperon, G. E.; Grancini, G.; Menelaou, C.; Alcocer, M.; Leijtens, T.; Herz, L. M.; Petrozza, A.; Snaith, H. J. *Science*, **2013**, *342*, 341-344.
6 Heo, J. H.; Im, S. H.; Noh, J. H.; Mandal, T. N.; Lim, C. S.; Chang, J. A.; Lee, Y. H.; Kim, H. J.; Sarkar, A.; Nazeeruddin, M. K.; Gratzel, M.; Seok, S. I. *Nat. Photon.*, **2013**, *7*, 487-492.
7 Burschka, J.; Pellet, N.; Moon, S. J.; Humphry-Baker, R.; Gao, P.; Nazeeruddin, M. K.; Gratzel, M. *Nature*, **2013**, *499*, 316 – 319.
8 Liu, M. Z.; Johnston, M. B.; Snaith, H. J. *Nature*, **2013**, *501*, 395-398.
9 Zhou, H. P.; Chen, Q.; Li, G.; Luo, S.; Song, T. B.; Duan, H. S.; Hong, Z. R.; You, J. B.; Liu, Y. S.; Yang, Y. *Science*, **2014**, *345*, 542-546.
10 Park, N. G. *J. Phys. Chem. Lett.*, **2013**, *4*, 2423-2429.
11 Green, M. A.; Ho-Baillie, A.; Snaith, H. J. *Nat. Photon.*, **2014**, *8*, 506-514.
12 Chen, Q.; Zhou, H. P.; Hong, Z. R.; Luo, S.; Duan, H. S.; Wang, H. H.; Liu, Y. S.; Li, G.; Yang, Y. *J. Am. Chem. Soc.*, **2014**, *136*, 622-625.
13 Abate, A.; Leijtens, T.; Pathak, S.; Teuscher, J.; Avolio, R.; Errico, M. E.; Kirkpatrik, J.; Ball, J. M.; Docampo, P.; McPherson, I.; Snaith, H. J. *Phys. Chem. Chem. Phys.*, **2013**, *15*, 2572-2579.
14 Haque, S. A.; Tachibana, Y.; Willis, R. L.; Moser, J. E.; Gratzel, M.; Klug, D. R.; Durrant, J. R. *J. Phys. Chem. B*, **2000**, *104*, 538-547.
15 Kopidakis, N.; Benkstein, K. D.; van de Lagemaat, J.; Frank, A. J. *J. Phys. Chem. B*, **2003**, *107*, 11307-11315.
16 Nakade, S.; Kanzaki, T.; Kubo, W.; Kitamura, T.; Wada, Y.; Yanagida, S. *J. Phys. Chem. B*, **2005**, *109*, 3480-3487.
17 Katoh, R.; Kasuya, M.; Kodate, S.; Furube, A.; Fuke, N.; Koide, N. *J. Phys. Chem. C*, **2009**, *113*, 20738-20744.
18 Koops, S. E.; O'Regan, B. C.; Barnes, P.; Durrant, J. R. *J. Am. Chem. Soc.*, **2009**, *131*, 4808-4818.
19 Abate, A.; Hollman, D. J.; Teuscher, J.; Pathak, S.; Avolio, R.; D'Errico, G.; Vitiello, G.; Fantacci, S.; Snaith, H. *J. Am. Chem. Soc.*, **2013**, *135*, 13538-13548.
20 Zhang, H.; Shi, Y. T.; Yan, F.; Wang, L.; Wang, K.; Xing, Y. J.; Donga, Q. S.; Ma, T. L. *Chem. Comm.*, **2014**, *50*, 5020-5022.
21 Xu, B.; Huang, J.; AA Gren, H.; Kloo, L.; Hagfeldt, A.; Sun, L. *ChemSusChem*, **2014**, *7*, 3252-3256.
22 OHZUKU, T.; UEDA, A.; YAMAMOTO, N. *J. Electrochem. Soc.*, **1995**, *142*, 1431-1435.
23 Aldon, L.; Kubiak, P.; Womes, M.; Jumas, J. C.; Olivier-Fourcade, J.; Tirado, J. L.; Corredor, J. I.; Vicente, C. P. *Chem. Mat.*, **2004**, *16*, 5721-5725.
24 Nakazawa, T.; Grismanovs, V.; Yamaki, D.; Katano, Y.; Aruga, T. *Nucl. Instrum. Methods Phys. Res. Sect. B-Beam Interact. Mater. Atoms*, **2003**, *206*, 166-170.
25 Ronci, F.; Reale, P.; Scrosati, B.; Panero, S.; Albertini, V. R.; Perfetti, P.; di Michiel, M.; Merino, J. M. *J. Phys. Chem. B*, **2002**, *106*, 3082-3086.
26 Dedryvere, R.; Foix, D.; Franger, S.; Patoux, S.; Daniel, L.; Gonbeau, D. *J. Phys. Chem. C*, **2010**, 114, 10999-11008.
27 Fantacci, S.; De Angelis, F.; Nazeeruddin, M. K.; Gratzel, M. *J. Phys. Chem. C*, **2011**, *115*, 23126-23133.
28 Cappel, U. B.; Daeneke, T.; Bach, U. *Nano Lett.*, **2012**, *12*, 4925-4931.
29 Wilkening, M.; Amade, R.; Iwaniak, W.; Heitjans, P. *Phys. Chem. Chem. Phys.*, **2007**, *9*, 1239-1246.
30 Bisquert, J. *Phys. Chem. Chem. Phys.*, **2003**, *5*, 5360-5364.
31 Fabregat-Santiago, F.; Garcia-Belmonte, G.; Mora-Sero, I.; Bisquert, J. *Phys. Chem. Chem. Phys.*, **2011**, *13*, 9083-9118.
32 Kim, H. S.; Mora-Sero, I.; Gonzalez-Pedro, V.; Fabregat-Santiago, F.; Juarez-Perez, E. J.; Park, N. G.; Bisquert, J. *Nat. Commun.*, **2013**, *4*.
33 Li, W. Z.; Dong, H. P.; Wang, L. D.; Li, N.; Guo, X. D.; Li, J. W.; Qiu, Y. *J. Mater. Chem. A*, **2014**, *2*, 13587-13592.
34 Shi, J. J.; Dong, W.; Xu, Y. Z.; Li, C. H.; Lv, S. T.; Zhu, L. F.; Dong, J.; Luo, Y. H.; Li, D. M.; Meng, Q. B.; Chen, Q. *Chin. Phys. Lett.*, **2013**, *30*, 128402.
35 Ouyang, C. Y.; Zhong, Z. Y.; Lei, M. S. *Electrochem. Commun.*, **2007**, *9*, 1107-1112.
36 Kim, H. S.; Lee, J. W.; Yantara, N.; Boix, P. P.; Kulkarni, S. A.; Mhaisalkar, S.; Gratzel, M.; Park, N. G. *Nano Lett.*, **2013**, 13, 2412-2417.
37 Juarez-Perez, E. J.; Wussler, M.; Fabregat-Santiago, F.; Lakus-Wollny, K.; Mankel, E.; Mayer, T.; Jaegermann, W.; Mora-Sero, I. *J. Phys. Chem. Lett.*, **2014**, 5, 680-685.
38 Lv, S. T.; Han, L. Y.; Xiao, J. Y.; Zhu, L. F.; Shi, J. J.; Wei, H. Y.; Xu, Y. Z.; Dong, J.; Xu, X.; Li, D. M.; Wang, S. R.; Luo, Y. H.; Meng, Q. B.; Li, X. G. *Chem. Comm.*, **2014**, *50*, 6931-6934.
39 Christians, J. A.; Fung, R.; Kamat, P. V. *J. Am. Chem. Soc.*, **2014**, *136*, 758-764.

Journal of Materials Chemistry A Accepted Manuscript

Graphical and textual abstract

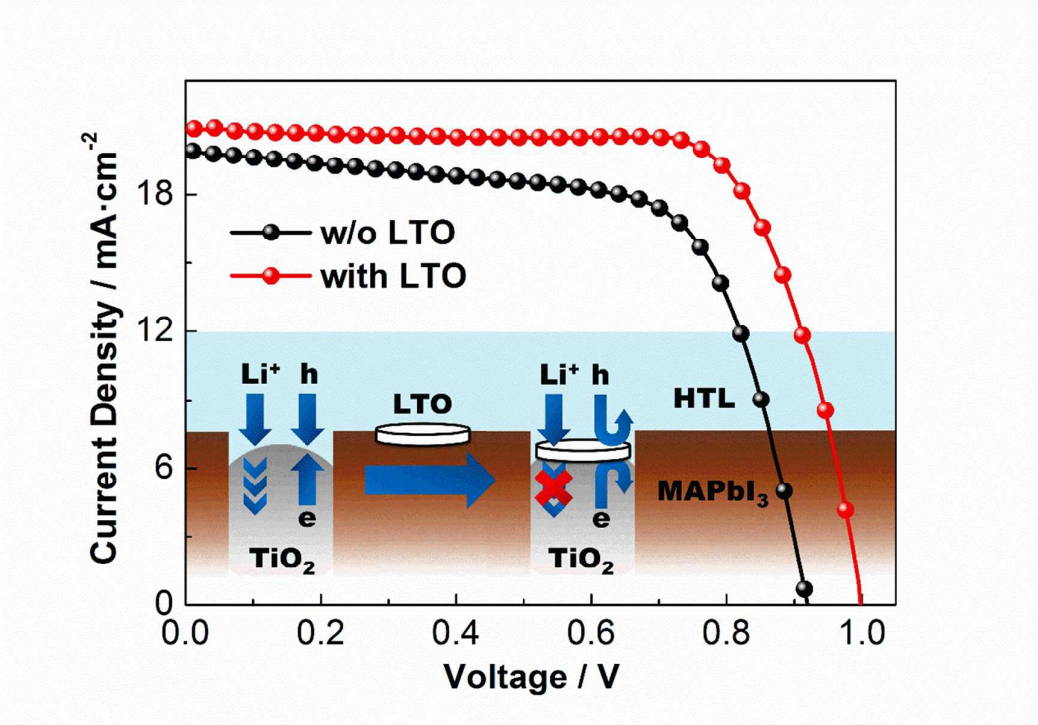

Spinel lithium titanate (LTO) was used as modification material at the perovskite-sensitized TiO_2/HTL interface, acting as a Li^+ separator to prevent Li^+ intercalation into TiO_2 and reducing carrier recombination.

Journal of Materials Chemistry A Accepted Manuscript